MED. INFORM. (SEPTEMBER 2003) VOL. 28, NO. 3, 221–230

Taylor&Francis
healthsciences

Support vector machines based analysis of brain SPECT images for determining cerebral abnormalities in asymptomatic diabetic patients

I. KALATZIS†, D. PAPPAS‡, N. PILIOURAS†
and D. CAVOURAS†*

†Department of Medical Instrumentation Technology, Technological Educational Institution of Athens, Ag. Spyridonos Street, Egaleo GR-122 10, Athens, Greece

‡Department of Nuclear Medicine, 251 General Airforce Hospital, Athens, Greece

(Received December 2002)

Abstract. *Purpose*: An image processing method was developed to investigate whether brain SPECT images of patients with diabetes mellitus type II (DMII) and no brain damage differ from those of normal subjects.
Materials and methods: Twenty-five DMII patients and eight healthy volunteers underwent brain 99mTc-Bicisate SPECT examination. A semi-automatic method, allowing for physician's interaction, was developed to delineate specific brain regions (ROIs) on the SPECT images. Twenty-eight features from the grey-level histogram and the spatial-dependence matrix were computed from numerous small image-samples collected from each specific ROI. Classification into 'diabetics' and 'non-diabetics' was performed for each ROI separately. The classical least squares-minimum distance (LSMD) classifier and the recently developed support vector machines (SVM) classifier were used. System performance was evaluated by means of the leave-one-out method; one sample was left out, the classifier was trained by the rest of the samples, and the left-out sample was classified. By repeating for all samples, the classifier's performance could be tested on data not incorporated in its design.
Results: Highest classification accuracies (LSMD: 97.8%, SVM: 99.1%) were achieved at the right occipital lobule employing two features, the standard deviation and entropy. For the rest of the ROIs classification accuracies ranged between 84.5 and 98.6%.
Conclusion: Our findings indicate cerebral blood flow disruption in patients with DMII. The proposed system may assist physicians in evaluating cerebral blood flow in patients with DMII undergoing brain SPECT.

Keywords: Diabetes mellitus type II; Brain SPECT examination; Computer-based classification

1. Introduction

Diabetes mellitus (DM) is a common disease in the industrialized countries and it is a prominent risk factor for ischaemic cerebrovascular accidents [1], diabetes alone being responsible for 7% of deaths in stroke patients [2]. Diabetes mellitus often results in brain micro-blood flow disorders that may cause cerebral infarction [3]. However, assessing the function of cerebral micro-vessels is difficult, since they are located within the bony skull [4]. Diagnostic methods employed for evaluating cerebral functionality are high resolution transcranial Doppler ultrasound (TCD), measuring blood flow velocity in the basal cerebral arteries at rest or after

*Author for correspondence; e-mail: cavouras@teiath.gr

Medical Informatics & The Internet in Medicine ISSN 1463-9238 print/ISSN 1464-5238 online © 2003 Taylor and Francis Ltd
http://www.tandf.co.uk/journals
DOI: 10.1080/1463923031000161344 9

administration of vasodilatory stimulus, and photon emission computed tomography (SPECT), utilizing perfusion agents such 99mTc-HMPAO and 99mTc-ECD for the assessment of cerebral micro-blood flow [4]. Previous studies by brain SPECT [5–11] have reported differences in the activity distribution between DM patients and normal subjects, while other studies [12–14] have reported no differences between the two groups.

In the present study we investigate whether brain SPECT images of patients with DM type II and no clinical indications of brain damage differ from those of healthy subjects by applying pattern recognition methods in evaluating cerebral blood flow than classical statistical significance tests employed in previous studies. For this, we have developed an automatic system for discriminating brain SPECT images of patients with DMII and healthy volunteers. The aim was to analyse the radio-pharmaceutical distribution in the brain as depicted on SPECT images, in order to investigate probable differences in cerebral blood flow between diabetics and non-diabetics. The count distribution was analysed by means of features derived from the SPECT image grey level histogram and grey level co-occurrence matrix [15]. These features evaluate the distribution of grey levels and the spatial relationships of the pixels in the image. The radio-pharmaceutical count information extracted from these features together with a classification algorithm, were used in the design of the image analysis system. Two different software classifiers were considered, the classical least squares-minimum distance (LSMD) classifier [16] and the recently developed support vector machine (SVM) classifier [17–20].

2. Material and methods

2.1. *Patient population*

Twenty-five patients with known diabetes mellitus type II (DMII) and with absence of clinical findings of brain damage were examined (10 women and 15 men, aged 40–65 years old, mean 53 $\pm$ 12 years). Eight healthy volunteers (three women and five men, aged 38–66 years old) were also examined, and included as normal controls.

2.2. *Examination procedure*

Each subject underwent brain SPECT 45 min after injection 20 mCi (740 MBq) of 99mTc-Bicisate (ECD). The radio-pharmaceutical was injected intravenously in a dimly lit quiet room. Following injection, the patients remained in the injection area for 10 min while the radiotracer was accumulated in the brain. Projections were acquired on a single-head DS7 Sophy gamma camera using a 360° rotation of the camera head resulting in 64 projection views of 25 s duration each. Transverse slices were reconstructed from the planar projections using filtered back-projection reconstruction algorithm with Butterworth order $n=5$, cut-off $=0.35$ pixel^{-1}. Attenuation correction was employed using the Chang method with linear coefficient equal to 0.12 cm^{-1}. No scatter correction was performed. Slices were oriented parallel to the meato-orbital line. The image matrix was 16-bit 128 × 128 pixels (pixel size x = 3.2 mm, y = 3.2 mm, z = 3.35 mm).

2.3. *Image segmentation*

Each SPECT image was segmented into regions of interest (ROI) [21] by means of a semi-automatic custom designed method that we especially developed

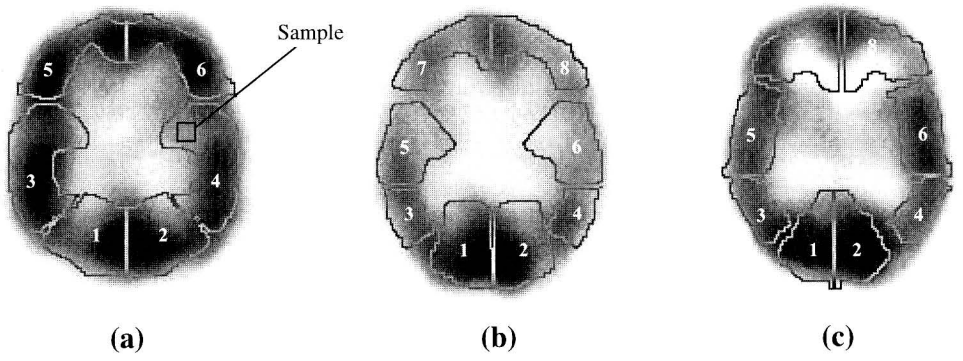

Figure 1. Three brain SPECT transverse slices (a), (b), and (c), segmented into regions of interest (ROIs). Each ROI was automatically divided into numerous small square image-samples, such as in (a).

(in C++) on a workstation to fit transverse slices of varying sizes (figure 1). Each ROI was automatically drawn by the software on the SPECT image to fit approximately a specific anatomical area of the brain. To ensure anatomical accuracy in the segmented regions, the software allowed for fine-tuning, which was performed interactively by the physician. However, accuracy was affected by the SPECT's spatial resolution and by the physician's interaction. Each ROI was next automatically divided by the software into small square areas (samples), as the one shown in figure 1a. This provided for more representative features used in the design of the classifiers, due to considerable variations in activity distribution within each ROI. Thus, a large number of 'diabetics' and 'non-diabetics' image-samples were formed for each ROI, which were used for further processing and analysis. The size of the image-sample was chosen by trial-and-error to be 12 × 12 pixels, to contain sufficient activity information without considerable variation in activity distribution.

2.4. *Feature generation*

From each one of the image-samples, features evaluating radio-pharmaceutical uptake distribution were extracted by means of first- and second-order statistics [15, 22, 23]. The first-order statistics were derived from the image-sample grey-level distribution (histogram) and they comprised the mean, standard deviation, skewness, and kurtosis. The grey-level histogram is a function describing the frequency of appearance of the grey-levels in the image-sample and, if $I(x,y)$ is an $N_x \times N_y$ image-sample, with $x = 1,2\ldots,N_x$ and $y = 1,2\ldots,N_y$, it is formally given by:

$$h(g) = \#\{(x,y) : I(x,y) = g\} \tag{1}$$

where # denotes the number of elements in the set, and $g = 0,1,2,\ldots,N_g - 1$, where N_g represents the number of grey-levels in the image-sample.

Regarding the second-order statistics, 12 features were computed from the co-occurrence matrix [15] using one pixel step length. Each second-order statistic feature was represented by two values, the mean and range over the 0°, 45°, 90° and 135° co-occurrence matrices, to ensure rotation independence. The co-occurrence matrix is a two dimensional histogram that describes the frequency of occurrence

of all pairs of grey-levels at a relative displacement d in an image I(x,y). Its (i,j)-th element is formally given by [22]:

$$P_{\delta,\theta}(i,j) = \#\{((x_1,y_1),(x_2,y_2)) : f(x_1,y_1) = i,\ f(x_2,y_2) = j,\ x_2 = x_1 + \delta\cos\theta,\ y_1 = y_2 + \delta\sin\theta\} \quad (2)$$

where # denotes the number of elements in the set, and (δ,θ) are the polar co-ordinates of the displacement vector between (x_1,y_1) and (x_2,y_2). Features calculated from the co-occurrence matrix evaluate properties of image grey-level distribution, such as homogeneity, contrast, grey-level local variation, linear-dependencies, lack of order etc. In this way, a total of 28 features were calculated for each image-sample, four from the image-sample histogram and 24 from the co-occurrence matrix (in fact 12 features, each being represented by two values, the mean and range). Ideally, these features should be employed in the design of the classifier, but since a number of them may be redundant due to mutual correlations [23], an optimum number of them has to be selected to achieve highest classification accuracy.

2.5. *Feature selection and classification*

Best feature selection was based on the performance of the classifier. The accuracy of classification was evaluated exhaustively by combining features in all possible ways (e.g. 2, 3, 4 combinations) to design the classifier. The aim was to determine the highest classification accuracy with the minimum number of features. In the present study, highest classification accuracy was achieved by two features, the standard deviation, describing local grey-level variation, and entropy, showing lack of order in grey-level distribution.

The standard deviation was calculated by means of equation (3):

$$\mathrm{SD} = \left(\frac{1}{\mathrm{N_x} \cdot \mathrm{N_y}} \sum_{\mathrm{x}=1}^{\mathrm{N_x}} \sum_{\mathrm{y}=1}^{\mathrm{N_y}} (\mathrm{I(x,y)} - \mu_{\mathrm{g}})^2 \right)^{\frac{1}{2}} \quad (3)$$

where μ_g is the mean grey-level of the image:

$$\mu_g = \frac{1}{N_x \cdot N_y} \sum_{x=1}^{N_x} \sum_{y=1}^{N_y} I(x,y) \quad (4)$$

Entropy was determined by formula (5):

$$\mathrm{ENT} = -\sum_{i=0}^{N_g-1} \sum_{j=0}^{N_g-1} P(i,j)\ln(P(i,j)) \quad (5)$$

where $P(i,j)$ is defined in (2).

Classifier performance was evaluated by means of the leave-one-out method [23], and results were presented in truth tables that revealed the classifier's discriminatory ability in distinguishing between 'diabetics' and 'non-diabetics' image-samples. Classification between the two groups was performed for each ROI separately, to map probable differences in count distribution between the two groups. Two software classifiers were employed for comparison reasons, the classical least

squares-minimum distance (LSMD) classifier [16], and the recently developed support vector machines (SVM) classifier [17–20].

For the LSMD, the discriminant function for class i and for pattern vector $\mathbf{x}$ is given by:

$$g_i(\mathbf{x}) = \sum_{j=1}^{d} \alpha_{ij} x_j - b_i \tag{6}$$

where d is the number of features, α_{ij} are weight elements, b_i is a threshold parameter, and x_j are the pattern vector elements.

The weight elements α_{ij} and the threshold parameter b_i are calculated by mapping first the patterns from the *feature* space in a K-dimensional space (*decision* space), where K is the number of classes. In the decision space, the members of each class are clustered around arbitrary pre-selected points, such that the mapping error (as expressed by the total mean-square error between the training set and the arbitrary selected points) is minimized.

Regarding SVM, the discriminant equation is a function of kernel $k(\mathbf{x}_i,\mathbf{x})$ and, for the case of two classes, is given by:

$$g(\mathbf{x}) = \text{sign}\left(\sum_{i=1}^{N_s} \alpha_i y_i k(\mathbf{x}_i, \mathbf{x}) + b\right) \tag{7}$$

where a_i are weight elements, b is a threshold parameter, $\mathbf{x}_i$ are the support vectors (i.e. the pattern vectors that have their corresponding weights $a_i \neq 0$), N_S is the number of the support vectors, and $y_i \in \{-1, +1\}$ depending on the class.

For the case of two classes, the weight parameters α_i and the bias parameter b are calculated by finding two hyperplanes that fulfill the following conditions: (i) maximize the area between the hyperplanes (also called the *margin*); and (ii) minimize the number of patterns that lie between the hyperplanes. A third hyperplane through the middle of the margin is the decision boundary of the two classes.

In the present study the 2nd-degree polynomial function was used as kernel, given by $k(\mathbf{x},\mathbf{y}) = (\mathbf{x} \cdot \mathbf{y} + 1)^d$ where $d = 2$, resulting in the following discriminant function for the SVM classifier:

$$g(\mathbf{x}) = \text{sign}\left(\sum_{i=1}^{N_s} \alpha_i y_i (\mathbf{x}_i \cdot \mathbf{x} + 1)^2 + b\right) \tag{8}$$

Other kernels were also tested, such as the linear or the Gaussian radial basis function (RBF), but resulted in lower classification accuracy. RBF's lower precision, employing the leave-one-out method, was due to overfitting.

Results and discussion

Evaluating probable changes in the function of cerebral micro-vessels in patients with DMII and no clinical evidence of brain damage, may be of value in patient management. When such patients undergo brain SPECT, radiopharmaceutical uptake and distribution may contain valuable information, which may not be clearly evident by visual inspection. However, if the count distribution as depicted on SPECT images is examined by computer image analysis methods,

utilizing features that are difficult to perceive visually, useful information concerning cerebral blood flow changes may be revealed.

In the present study, a number of features, stemming from the grey level histogram (first-order statistics) and from the co-occurrence matrices (second-order statistics) were generated from image-samples of the SPECT images and were tested for their discriminatory power in distinguishing patients with DMII from normal controls. A representative example is shown in figure 2, which shows a plot of two features commonly employed by physicians in everyday practice in assessing SPECT images visually, namely mean value and standard deviation. As it can be seen from figure 2, there is a significant overlap between 'diabetics' and 'non-diabetics', which actually reflects the fact that visual inspection of SPECT images by the physicians may lead to no conclusive evidence of differences between the two groups of subjects. When, however, a co-occurrence matrix feature, namely entropy, was plotted against the standard deviation (figure 3a), the two groups were clearly separated, with an insignificant degree of overlap. Entropy signifies the lack of order in the grey-level distribution and as it can be observed in figure 3a, entropy attained higher values in diabetic patients than in non-diabetics. This may lead to the assumption that micro-blood flow in diabetics is unevenly distributed, in comparison to the healthy subjects.

The highest classification accuracy with the minimum number of features was achieved for the feature combination 'standard deviation–mean entropy' in the area of the cuneus at the right occipital lobule (region 1 in figure 1). The LSMD classifier (see table 1) classified correctly all 'non-diabetics' image-samples (167/167) and 53 out of 58 'diabetics' image-samples giving an overall accuracy of

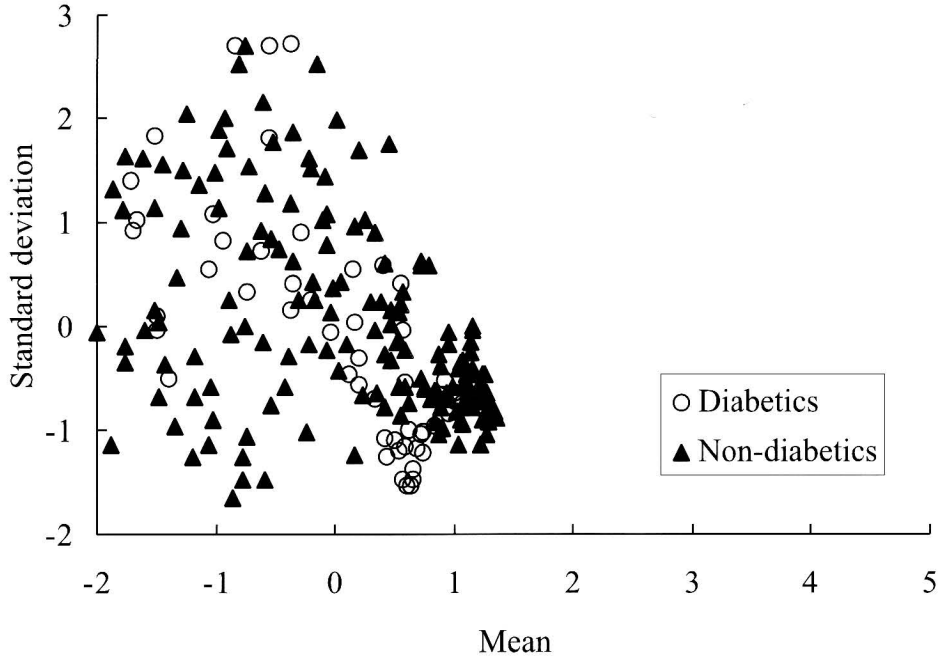

Figure 2. 'Standard deviation–Mean' plot (normalized values) corresponding to the right occipital lobule (region 1 in Figure 1(c)).

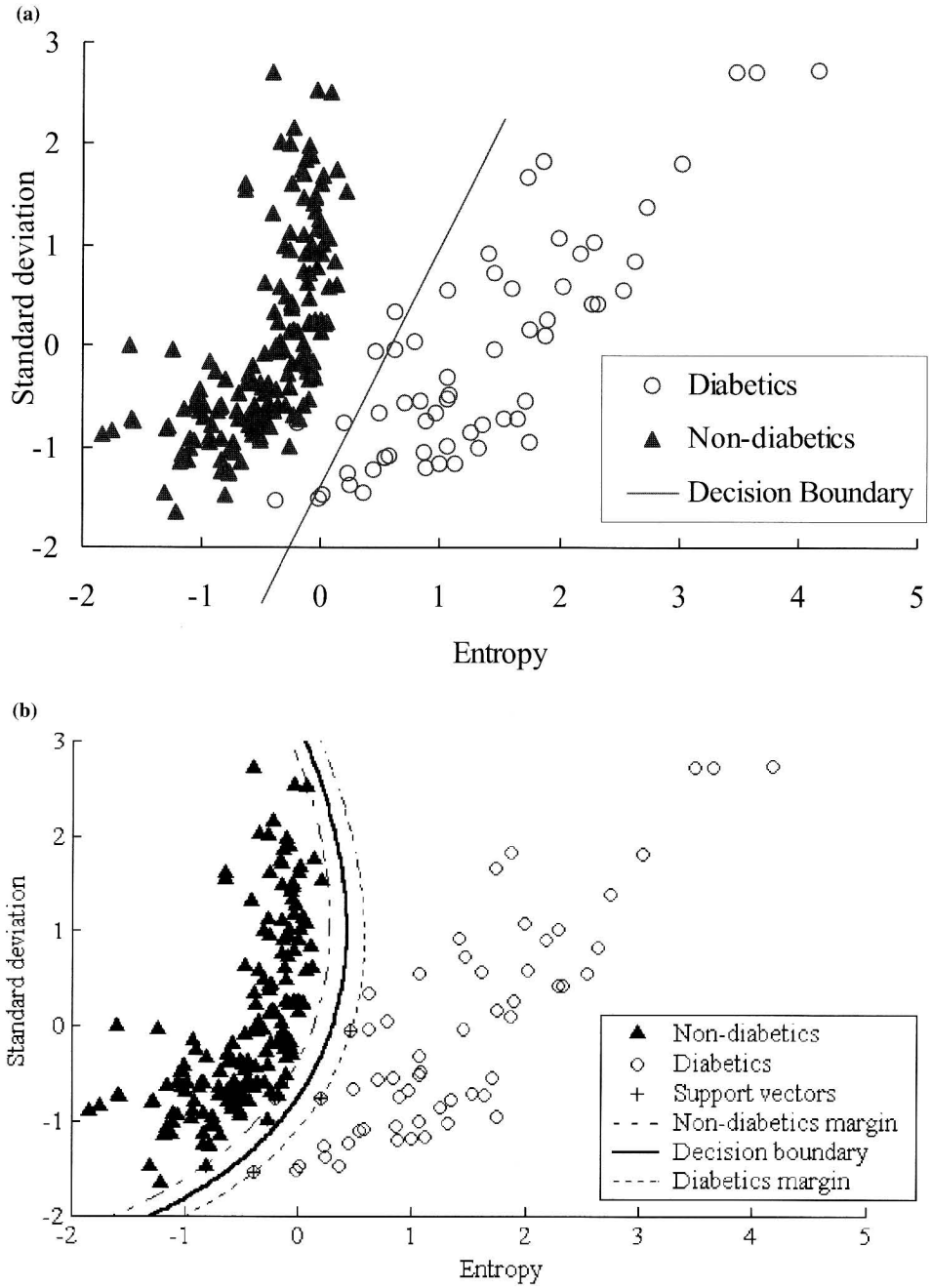

Figure 3. 'Standard deviation–Entropy' plots (normalized values) and decision boundaries drawn by (a) the LSMD classifier and (b) the SVM classifier, for the ROI corresponding to the right occipital lobule.

97.8% (220/225). The fact that the five 'diabetics' image-samples were misclassified as 'non-diabetics' is probably indicative that DMII in asymptomatic patients does not always induce changes in micro-vessel function that could affect brain blood

Table 1. Truth table demonstrating LSMD classification of samples corresponding to the right occipital lobule of diabetics and non-diabetics using the best feature combination (standard deviation–entropy).

	LSMD classification		
Patient group	Diabetics	Non-diabetics	Accuracy
Non-diabetics	0	167	100%
Diabetics	53	5	91.4%
Overall accuracy			97.8%

Table 2. Truth table demonstrating SVM classification of samples corresponding to the right occipital lobule of diabetics and non-diabetics using the best feature combination (standard deviation–entropy).

	SVM classification		
Patient group	Diabetics	Non-diabetics	Accuracy
Non-diabetics	0	167	100%
Diabetics	56	2	96.6%
Overall accuracy			99.1%

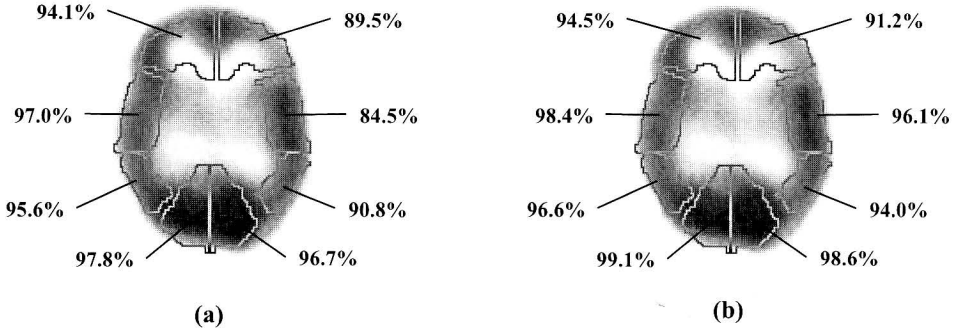

Figure 4. Classification accuracies achieved in different ROIs by (a) the LSMD and (b) the SVM classifiers.

flow. The SVM classifier (see table 2) classified correctly all 'non-diabetics' image-samples (167/167) and 56 out of 58 'diabetics' image-samples giving an overall accuracy of 99.1% (223/225). When comparing these results (tables 1 and 2), the SVM classifier, due to its non-linear nature of the kernel used (2nd-degree polynomial), outperformed the LSMD by classifying correctly all normals and missing out only two 'diabetics' samples, which are situated well within the group distribution of the non-diabetics in figure 3b.

In the rest of the ROIs, overall accuracies in correctly discriminating between 'diabetics' and 'non-diabetics' image-samples varied between 84.5% and 98.6% as indicatively shown in figure 4. Indications that differences in cerebral brain function between diabetics and normals may exist have also been reported by previous workers, although their findings are contradicting. In a previous study [24] employing brain SPECT images of patients with DM type II, the average regional

cerebral brain function in the cerebrum and cerebellum was significantly lower in diabetics than in non-diabetics, even in the absence of findings indicative of cerebral infarction on a CT study. In an other study concerning DMII [25], patients without previous history of cerebrovascular disease showed subclinical cerebral abnormalities on brain magnetic resonance imaging. In contrast, a previous study [4] found no differences between DMII patients and non-diabetics in measurements of the resting cerebral blood flow velocity, employing brain SPECT.

In conclusion, our findings indicate the existence of differences in brain activity distribution between patients with DMII and normal subjects. These differences were found by evaluating count distribution features from the brain SPECT images, such as entropy, that are not easily discernable by visual inspection. The usefulness of the present system is its ability to semi-automatically segment ROIs on brain SPECT images and then provide physicians with a second opinion concerning changes in brain activity distribution of patients with DMII. Its final testing ground will be the clinical environment, where many new cases of DMII will be presented.

References

1. CHUKWUMA, C. and TUOMILEHTO J., 1993, Diabetes and the risk of stroke. *Journal of Diabetes and Its Complications*, **7**, 250–262.
2. BOGOUSSLAVSKY, J., 1999, Stroke prevention by the practitioner. *Cerebrovascular Diseases*, **9**, 19–22.
3. KANNEL, W. B. and MCGEE, D. L., 1979, Diabetes and cardiovascular disease. The Framingham study. *Journal of the American Medical Association*, **241**, 2035–2038.
4. FULESDI, B., LIMBURG, M., BERECZKI, D., KAPLAR, M., MOLNAR, C., KAPPELMAYER, J., NEUWIRTH, G. and CSIBA, L., 1999, Cerebrovascular reactivity and reserve capacity in type II diabetes mellitus. *Journal of Diabetes and Its Complications*, **13**(4), 191–199.
5. JIMENEZ-BONILLA, J. F., CARRIL, J. M., QUIRCE, R., GOMEZ-BARQUIN, R., AMADO, J. A. and GUTIERREZ-MENDIGUCHIA, C., 1996, Assessment of cerebral blood flow in diabetic patients with no clinical history of neurological disease. *Nuclear Medicine Communications*, **17**(9), 790–794.
6. KASHIHARA, K., SHOHMORI, T. and OTSUKI, S., 1997, Noninsulin-dependent diabetes mellitus-related encephalopathy presenting with amnesia, personality change, and autonomic seizure. *Internal Medicine*, **36**(9), 633–636.
7. KEYMULEN, B., DE METZ, K., CLUYDTS, R., BOSSUYT, A. and SOMERS, G., 1996, Technetium-99m hexamethylpropylene amine oxime single-photon emission tomography of regional cerebral blood flow in insulin-dependent diabetes. *European Journal of Nuclear Medicine*, **23**, 163–168.
8. KEYMULEN, B., JACOBS, A., DE METZ, K., DE SADELEER, C., BOSSUYT, A. and SOMERS, G., 1995, Regional cerebral hypoperfusion in long-term type 1 (insulin-dependent) diabetic patients: relation to hypoglycemic events. *Nuclear Medicine Communications*, **16**, 10–16.
9. MANKOVSKY, B. N., METZGER, B. E., MOLITCH, M. E. and BILLER, J., 1996, Cerebrovascular disorders in patients with diabetes mellitus. *Journal of Diabetes and Its Complications*, **10**(4), 228–242.
10. QUIRCE, R., CARRIL, J. M., JIMENEZ-BONILLA, J. F., AMADO, J. A., GUTIERREZ-MENDIGUCHIA, C., BANZO, I., BLANCO, I., URIARTE, I. and MONTERO, A., 1997, Semi-quantitative assessment of cerebral blood flow with 99mTc-HMPAO SPET in type I diabetic patients with no clinical history of cerebrovascular disease. *European Journal of Nuclear Medicine*, **24**, 1507–1513.
11. WAKISAKA, M., NAGAMACHI, S., INOUE, K., MOROTOMI, Y., NUNOI, K. and FUJISHIMA, M., 1990 Reduced regional cerebral blood flow in aged noninsulin-dependent patients with no history of cerebrovascular disease. Evaluation by N-isopropyl-l123-p-iodoamphetamine with single-photon emission computed tomography. *Journal of Diabetes and Its Complications*, **4**, 170–174.
12. RODRIGUEZ, G., NOBILI, F., CELESTINO, M. A., FRANCIONE, S., GULLI, G., HASSAN, K., MARENCO, S., ROSADINI, G. and CORDERA, R., 1993, Regional cerebral blood flow and cerebrovascular reactivity in IDDM. *Diabetes Care*, **16**(2), 462–468.
13. SABRI, O., HELLWIG, D., SCHRECKENBERGER, M., SCHNEIDER, R., KAISER, H. J., WAGENKNECHT, G., MULL, M. and BUELL, U., 2000, Influence of diabetes mellitus on regional cerebral glucose metabolism and regional cerebral blood flow. *Nuclear Medicine Communications*, **21**(1), 19–29.
14. TERAI, T., SYOMORI, T., HIMEI, H. and MATSUOKA, T., 1993, Cerebral blood flow disorder in elderly patients with diabetes mellitus. *No To Shinkei*, **45**(10), 945–949.

15. HARALICK, R. M., SHANMUGAM, K. and DINSTEIN, I.'H., 1973, Textural features for image classification. *IEEE Transactions on System, Man, and Cybernetics*, **6,** 610–621.
16. AHMED, N. and RAO, K. R., 1975, Orthogonal Transforms for Digital Signal Processing, (New York: Springer-Verlag), pp. 225–258.
17. BURGES, C. J. C., 1998, A tutorial on support vector machines for pattern recognition. *Data Mining and Knowledge Discovery*, **2**(2), 1–32.
18. KECMAN, V., 2001, *Learning and Soft Computing, Support Vector Machines, Neural Networks, and Fuzzy Logic Models*, (Cambridge, MA: MIT Press), pp. 121–191.
19. MULLER, K.-R., MIKA, S., RATSCH, G., TSUDA, K. and SCHOLKOPF, B., 2001, An introduction to kernel-based learning algorithms. *IEEE Transactions on Neural Networks*, **12**(2), 181–202.
20. PLATT, J. C., 1999, Sequential minimal optimization: a fast algorithm for training support vector machines. In *Advances in Kernel Methods–Support Vector Learning*, edited by B. Schölkopf, C. J. C. Burges and A. J. Smola, (Cambridge, MA: MIT Press), pp. 185–208.
21. PARTENSTEIN, P., LUDOLPH, A., SCHOBER, O., LOTTES, G., SCHEIDHAUER, K., JOACHIM, S. and BEER, H.-F., 1991, Benzodiazepine receptors and cerebral blood flow in partial epilepsy. *European Journal of Nuclear Medicine*, **18,** 111–118.
22. BOCCHI, L., COPPINI, G., DE DOMINICIS, R. and VALLI, G., 1997, Tissue characterization from X-ray images. *Medical Engineering and Physics*, **19**(4), 336–342.
23. THEODORIDIS, S. and KOUTROUMBAS, K., 1998, System evaluation. In *Pattern Recognition*. (London: Academic Press), pp. 342–343.
24. NAGAMACHI, S., NISHIKAWA, T., ONO, S., AGETA, M., MATSUO, T., JINNOUCHI, S., HOSHI, H., OHNISHI, T., FUTAMI, S. and WATANABE, K., 1994, Regional cerebral blood flow in diabetic patients: evaluation by N-isopropyl-123I-IMP with SPECT. *Nuclear Medicine Communications*, **15,** 455–460.
25. INOUE, T., FUSHIMI, H., YAMADA, Y., UDAKA, F. and KAMEYAMA, M., 1996, Asymptomatic multiple lacunae in diabetics and non-diabetics detected by brain magnetic resonance imaging. *Diabetes Research and Clinical Practice*, **31,** 1–3.